Biointerface Research in Applied Chemistry
Platinum Open Access Journal (ISSN: 2069-5837)

Article
Volume 12, Issue 6, 2022, 7478 - 7487
https://doi.org/10.33263/BRIAC126.74787487

Thickness Variation Effects on the Efficiency of Simulated Hybrid Cu_2ZnSnS_4-Based Solar Cells Using SCAPS-1D

Ismaila Taiwo Bello [1,2,*], David Omoefe Idisi [1], Kamaldeen Olasunkanmi Suleman [2,3], Yetunde Ajayeoba [2,4], Oluwaseun Adedokun [2,*], Ayodeji Oladiran Awodugba [2], Mokhotjwa Simon Dhlamini [1]

1 Department of Physics, CSET, University of South Africa, Johannesburg 1710, South Africa; ismailbello26@gmail.com (I.T.B.); efedave26@gmail.com (D.O.I.); dhlamms@unisa.ac.za (M.S.D.);
2 Department of Pure and Applied Physics, Ladoke Akintola University of Technology, Ogbomoso, Nigeria. oadedokun@lautech.edu.ng (O.A); aoawodugba@lautech.edu.ng (A.O.A.);
3 Nigeria Maritime University, Okerenkoko, Delta State, Nigeria. kosuleman@lautech.edu.ng (K.O.S.);
4 Department of Physics, Osun State University, Osogbo, 210001, Nigeria. yetundeodedunmoye@gmail.com (Y.A.);
* Correspondence: ismailbello26@gmail.com (I.T.B); oadedokun@lautech.edu.ng (O.A);

Scopus Author ID 57202357845 (I.T.B); 57190128209 (O.A.)

Received: 5.10.2021; Revised: 7.11.2021; Accepted: 10.11.2021; Published: 25.11.2021

Abstract: This study presents the simulations of a hybrid Cu_2ZnSnS_4-based solar cell with a planar heterojunction structure in a hybrid model (n-FTO/n-ZnO/p-PSCS/p-CZTS/p-PSCS/p-HTM) using a One-Dimensional Solar cell capacitance simulator (SCAPS-1D). . The configuration "121" of the hybridizing absorber layers of the device was simulated and related with as-Copper Zinc Tin Sulphide (CZTS). The simulation used an absorber layer with a step-length thickness of 25 nm and thicknesses ranging from 100 nm to 500 nm. The bandgap diagram, I-V characteristics curve, percentage conversion efficiencies, and the quantum efficiencies of the simulated solar cells were calculated and constructed from simulated results. The percentage conversion efficiency of 22.57%, fill factor of 49.99%, open-circuit voltage of 0.80V, and short circuit current of 25.12 $mAcm^{-2}$ were obtained. The obtained photon conversion efficiency shows that the hybridization of different absorber layers was achievable. It was also established that the performance efficiencies of hybrid CZTS structure in terms of optimum thickness and sandwiched Perovskite Solar cells model (FTO/ZnO/CZTS/PSCS/CZTS/HTM) has the same efficiencies for "121 configurations". On the other hand, the efficiencies of as- CZTS structures were higher than the PSCS configuration, which might be due to SCAPS-1D as it was originally designed for Thin Films Solar cells.

Keywords: CZTS; hybrid; efficiency; modeling; thin film; solar cell.

1. Introduction

Fossil fuels account for more than 85% of the global total energy supply usage, ranging from transportation, industrial, domestic, and power plant purposes. Global warming and climate change have been caused by the uncontrolled usage of fossil fuels, increasing greenhouse gases in the atmosphere [1]. Consumption of these fuels should be decreased and managed, primarily by replacing them with less damaging and renewable energy sources at accessible, equivalent, or acceptable costs, to restore a stable and healthy environment for a better life and sustainable growth [2,3]. Solar energy is the most abundant and accessible renewable energy source, with the fewest negative side effects [4–6]. The main challenge with

using this energy source is that it requires a unique setup consisting of a light-harvesting device coupled to a transducer that converts the acquired optical energy to electric current and the collection and conduction of the created electrons [7–9]. A photovoltaic or solar cell is a system that can be used to harvest solar energy radiation from the sun. Basic parameters like efficiency, availability, and price of essential raw materials, production costs (of setup preparation), cell lifetime, and any environmental dangers should all be considered when designing a practically stable, functional, and commercially cost-effective solar cell [10].

Currently, a chalcogenide semiconductor compound of $Cu_2ZnSn\ (S_xSe_{1-x})_4$ (CZTSSe) has attracted a significant consideration in thin-film solar cells as an absorber layer because of its eco-friendly, availability, cost-effectiveness, and high efficiency in different applications [11–13]. The optical absorption coefficient of CZTS can be easily tuned due to the bandgap variation 1.4 – 1.6 eV, and their absorption spectroscopy is higher than $10^4\ cm^{-1}$ [14,15]. The bandgap tunability allows CZTS materials to absorb light with an absorber layer's thin thickness (1-2 μm). CZTS based thin films solar cells exhibit relatively weak conversion efficiencies of about 8.4% [16–18], compared to other reported technologically improved photovoltaics, like Copper-Indium-Gallium-Sulphide (CIGS) based solar cells that recorded efficiencies of over 20% [19]. Another attractive absorber material is a Perovskite material ($CH_3NH_3PbI_3$), which has attracted considerable attention as an absorbing layer. Perovskite solar cells (PSC) are highly efficient, low cost with improved output efficiency ranging from 3% to 20.1% [20–24]. PSC materials can be used in optoelectronic devices, electroluminescence from the visible to the near-infrared range, lasers, and photo-detector applications [25,26]. PSC materials naturally occur in a standard form of ABX_3 configuration, where A, B & X are organic cations, e.g., CH_3NH_{3+}, divalent metal cation, e.g., Pb_{+2}, Sn_{+2}, and halogen anion, e.g., Cl-, Br-, I-, respectively. It has a bandgap of about 1.55 eV, which can be increased by adding Cl or Br [25–27]. Although the lifespan of the cells has yet to be proven, there is no evidence that it is any longer or shorter than that of pure organic devices. The usage of lead in Perovskite compounds is unideal because there is the potential for a lead substitute to be used instead, and lead can be used in considerably smaller amounts than what is now used in lead or cadmium-based batteries. Finally, the optical density of Perovskite materials has yet to be extensively explored, even though it was lower than that of other active materials but higher than silicon. As a result, light-harvesting Perovskite devices require thicker layers, limiting the fabrication of solution-processed devices by making it difficult to achieve good uniformity with such thick layers [28,29]. Large-scale Atomic/Molecular Massively Parallel Simulator (LAMMPS), Silvaco ATLAS, Solar Cell Capacitance Simulator (SCAPS), and other simulation software models are used to simulate solar cells devices numerically.

In this research work, one dimensional Solar Cell Capacitance Simulator (SCAPS-1D) was employed to study the numerical simulation of the model due to the easy accessibility of the simulator and the reliability of the output results the simulations. The simulation of hybrid Cu_2ZnSnS_4-based solar cells was investigated vis-à-vis thickness variations. The multilayers' effect of thin-film (CZTS) and organometallic (Perovskite) on the efficiencies of the device were also investigated.

2. Materials and Methods

2.1. Device structure.

The cell model used in the simulation, Figure 1, is a stack of n-FTO/n-ZnO/p-PSC/p-CZTS/p-PSC/HTM multilayers. This cell structure consists of Fluorine doped tin Oxide (Sn_2O:F) as the transparent conductive layer, n-type ZnO layer as a buffer layer, Cu_2ZnSnS_4 (CZTS), and a Perovskite layer ($CH_3NH_3Pb_{3-x}Cl_x$), which is p-type.

Two different cells considered were "CZTS only" and hybrid "1:2:1" configuration cells, which connote PSC: CZTS: PSC with the initial ratio of "25: 50: 25" nm thicknesses in the absorber medium and subjected to a thickness variation in step length of 25 nm. The cell was illuminated with a transparent conductive oxide (TCO). The TCO serves as a window layer, which passes across the electron transport layer (n-type ZnO) and acts as a buffer layer, and enters the absorber layer to the hole transport material.

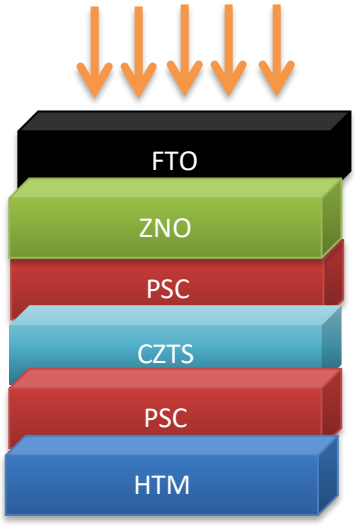

Figure 1. Model of Sandwiched Simulation structure.

2.2. Simulations.

SCAPS-1D simulator is based on the solutions of the three basic semiconductor equations; Poisson's equation, continuity equation of electron, and continuity equation of hole. SCAPS-1D software solves these three combined partial differential equations numerically for the electrostatic potentials' electron and hole concentrations as a function of positions x [30,31].

Poisson's equation is given as

$$\frac{\partial}{\partial x}\left(\varepsilon(x)\frac{\partial \psi}{\partial x}\right)=\frac{-q}{\varepsilon_0}\left[p-n+N_D^+-N_A^-+\frac{\rho_{def}(n,p)}{q}\right], \quad (1)$$

where ψ is electrostatic potential, ε is dielectric constant and q is the electronic charge, and ρ_{def} is defect charge density.

The conservation of free electrons and free holes in the device is expressed as continuity equations

$$\frac{\partial n}{\partial t}=-\frac{\partial J_n}{\partial n}+G-U_n(n,p), \quad (2)$$

$$\frac{\partial n}{\partial t} = -\frac{\partial J_p}{\partial x} + G - U_p(n, p), \quad (3)$$

where p, n represent free carrier concentrations, $N_{D,A}$ is for charged dopants, $\rho_{def}(n, p)$ for defects distributions, j_n, j_p is the electron and hole current densities, $U_{n,p}$ is the net recombination rates, and G is the generation rate.

The material parameters sourced from previously reported experiments [32,33] were used in this simulation, as given in Table 1. The absorption coefficient of the materials was determined based on the input parameter and model arrangement, as allowed by the SCAPS-1D simulator. The absorber layers were varied while the other parameters were kept constant. Various efficiencies were generated based on the thickness variation of the absorber.

All simulations in this work were performed under ambient temperature (300 K). The electrical parameters (V_{OC}, J_{SC}, FF) and efficiency generated by SCAPS-1D were used to determine the optimal thickness of the absorber layers in the two configurations. The simulation's current density – voltage (J-V) and quantum efficiency (Q.E) of the best solar cells were then determined. The influence of the sandwich on the absorber layer in the solar cell was investigated using material simulation parameters such as absorber layer thickness, bandgap, electron affinity, donor and acceptor densities, etc.

Table 1. Material parameters used in the simulation.

Parameters	FTO	ZnO	PSC	CZTS
Thickness (nm)	0.5	0.05	Varied	Varied
$E_g(eV)$	3.5	3.35	1.55	1.55
$X(eV)$	4.0	4.21	3.9	4.5
$\varepsilon_T(eV)$	9.0	9.0	6.5	10
$N_c(cm^{-3})$	2.2×10^{18}	2.2×10^{18}	2.2×10^{18}	2.2×10^{18}
$N_v(cm^{-3})$	1.8×10^{19}	1.8×10^{19}	1.8×10^{19}	1.8×10^{19}
$V_{\hat{o}}(cm/s)$	1.0×10^{7}	1.0×10^{7}	1.0×10^{7}	1.0×10^{7}
$V_h(cm/s)$	1.0×10^{7}	1.0×10^{7}	1.0×10^{7}	1.0×10^{7}
$\mu_e(cm^{-2}.V^{-1}s^{-1})$	2.0	25	1.6	100
$\mu_h(cm^{-2}.V^{-1}s^{-1})$	1.0	100	0.2	20
$N_D(cm^{-3})$	2.0×10^{19}	1.0×10^{18}	0	0
$N_A(cm^{-3})$	0	0	6.0×10^{18}	8.22×10^{18}

3. Results and Discussion

The band structure plot of solar cells hinges on the compositional variation of the constituent of the processing and synthesis of the absorber materials such as organic, metal, and anion composition of the material [34,35]. The bandgap of the absorbing material is a crucial parameter for photovoltaic actions, as the absorber layer is the key material in solar cells device [36]. Thus, the band alignment is the Type II Broken bandgap with approximately 1.55 eV, consistent with the theoretical reported values [37]. Figure 2 shows that the band alignment of CZTS thin-film solar cells describes a single junction bandgap, whereas the hybrid CZTS band gap shows three junctions, which confirms the presence of sandwiching encapsulation within the absorber layer.

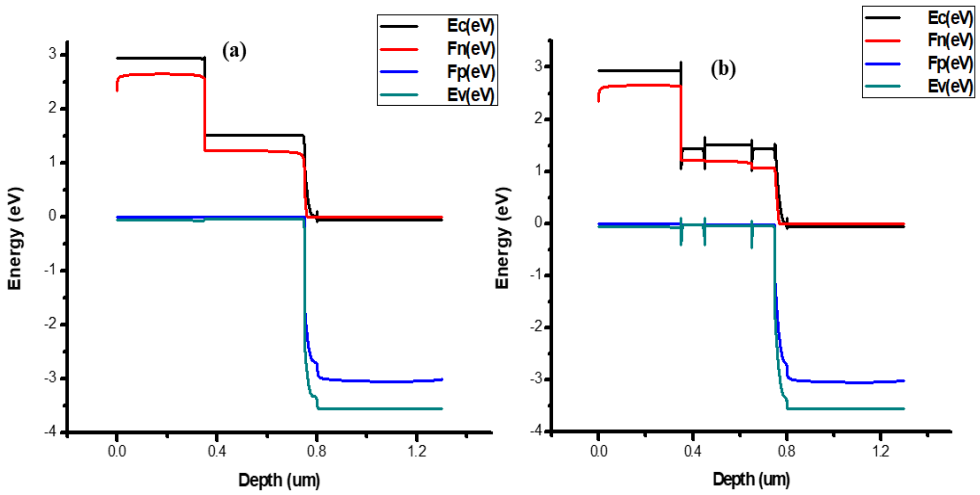

Figure 2. The band diagram of simulated hybrid devices.

3.1.$J-V$ characteristic of the simulated device.

$J-V$curves are the parameters used to calculate the electrical output power of solar cells. Figure 3 shows the $J-V$ curve of the hybrid simulated device, where, $V_{OC} = 0.80\,V$, $J_{SC} = 28.22\,mAcm^{-2}$, $FF = 49.99\%$ and, $PCE = 22.57\,\%$. These are cell output parameters under the standard simulated sunlight of AM1.5G. The working condition is at ambient temperature and frequency of 10^6 Hz.

3.2. Effect of sandwiched absorber layer configuration.

Solar cell device performance depends solely on the electrical characteristic and variation of the absorber layer thickness. From Figure 4, when the CZTS material thickness in the absorber layer was 100 nm, the efficiency of CZTS solar cells was 11.75%, whereas the efficiency of the hybrid CZTS was 16.12%, with a percentage increase of 37%. At 125 nm thickness, the efficiency of 13.42% was observed for CZTS, while 17.59% efficiency was observed for hybrid CZTS with a 31% increment. 14.81% efficiency was observed for CZTS solar cells, while 18.67% was observed for hybrid CZTS solar cells at 150 nm with a percentage increase of 26%. At 175 nm, the efficiency of 15.97% was observed for CZTS, while 19.48% efficiency was observed for hybrid CZTS cells with a percentage increase of 22%. Also, at 200 nm, 16.94% efficiency was observed for the CZTS cell, while the efficiency of 20.09% was observed for the "121" configuration with a percentage increase of 19%.

Meanwhile, 17.77% efficiency was recorded for CZTS cells, while 20.57% efficiency was observed at 225 nm for hybrid CZTS solar cells with a percentage increment of 16%. At 250 nm, an efficiency of 18.47% was observed for CZTS, and 20.95% efficiency was observed for hybrid CZTS cells with a percentage increase of 13%. The efficiency of 19.06% was observed for CZTS, while 21.26% efficiency was recorded for hybrid solar cells with a percentage increase of 12% at 275 nm thickness. At 300 nm, an efficiency of 19.57% was observed for CZTS solar cells, while 21.51% was observed for hybrid CZTS cells with a percentage increase of 10%. An efficiency of 20.01% was recorded for the CZTS cell at 325 nm, while the hybrid CZTS cell was observed to be 21.72%, with a percentage increase of 9%. At 350 nm, 20.39% efficiency was observed for CZTS, while 21.90% was observed for "121" hybrid CZTS with a percentage increase of 7%.

Meanwhile, at 375 nm, an efficiency of 20.72% was recorded for CZTS solar cells, while 22.05% was observed for hybrid CZTS with a percentage increase of 6%. Also, at 400 nm, efficiencies of 21.01% and 22.18% were recorded for both CZTS and hybrid CZTS solar cells with a percentage increase of 5.5%. At 425 nm, an efficiency of 21.27% was observed for the CZTS solar cell, while 22.30% was observed for the hybrid CZTS with a percentage increase of 5%. At 450 nm, 21.49% and 22.40% efficiencies were observed for CZTS and hybrid CZTS solar cells, respectively, with a percentage increase of 4%. However, 21.69% and 22.49% efficiencies were observed for both CZTS and hybrid CZTS, respectively, at 475 nm, with a percentage increase of 3.7%. Lastly, at 500 nm, the efficiency of CZTS was observed to be 21.86%, and that of hybrid CZTS was around 22.57%, with a percentage increase of 3%. Furthermore, there is no significant increment in the percentage increases of the efficiency values of sandwiched CZTS from the 375 nm thickness of the absorber layers. However, any further simulation beyond 500 nm in the "121" configuration failed as there was no convergence which implies that the configuration has large bandwidth, which affects the absorption processes to create electron-hole pairs for the excitation of photons. Further increase in the thickness (> 500 nm) was impossible due to the limit of computation. The computation limit signifies that the absorber layer thickness threshold limit is less than 500 nm for "121" configurations [38]. Meanwhile, the performance efficiency of the current study is consistent with previously reported values [28,38]. However, the efficiency values for the as-CZTS structure were higher than the PSC configuration. The difference may be due to the SCAPS-ID incompatibility.

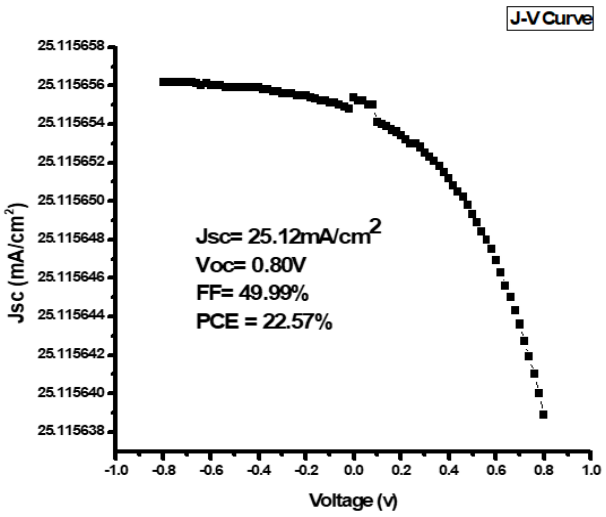

Figure 3. Hybrid $J-V$ curve characteristics.

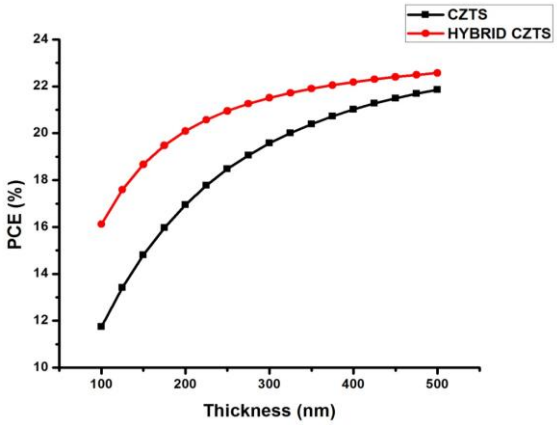

Figure 4. Sandwiched percentage conversion efficiency against thickness.

3.3. Quantum efficiency of the solar cell.

The ratio of the number of carriers collected by the solar cell to the number of photons of a given energy incident on the solar cell is known as quantum efficiency (Q.E.). It may also be given as either a function of wavelength or as energy. Figure 5 shows the plot of Quantum Efficiency against the wavelength, which showed that more than 90% of the wavelength between 300 nm and 890 nm radioactively recombined, and less than 10% of the wavelength recombined through other processes (Auger and SRH). This implied that, at 500 nm thickness, the sandwiched layer absorbs almost all the incident photons to create the electron-hole pairs and the photo-generated carriers by the built-in field with minimum recombination.

Figure 5, showed that the sandwiched layer could absorb incident photons up to 800 nm. This implies that the sandwiched absorber layer can perform better than the CZTS layer, which can only absorb photons around 750 nm, because the longer the wavelength, the lower the photon energy. Meanwhile, the flattering out of the curve at 800 nm shows that absorption beyond this region is unlikely.

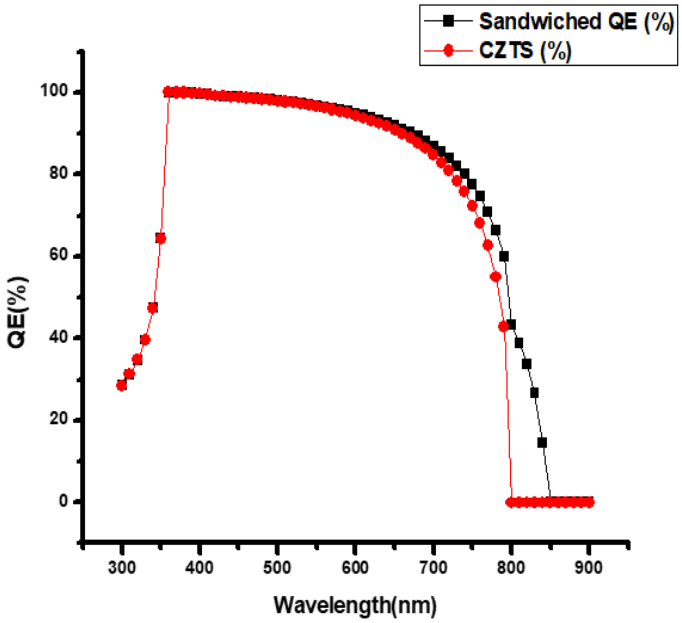

Figure 5. CZTS and HYBRID QE against wavelength.

4. Conclusions

Copper Zinc Tin Sulphide and Hybrid CZTS-Based solar cells were successfully simulated using a One-Dimensional Solar Cell Capacitance Simulator (SCAPS-1D). It was found that an increase in the absorber layer thickness range of 100 to 500 nm results in increased efficiency for hybrid CZTS (with optimum, 97% at 500 nm) in comparison to as-CZTS. Furthermore, it was established that higher absorber thickness (up to 400 nm) leads to higher efficiencies and other electrical output of the solar cells. The efficiencies of 21.86% and 22.57% were recorded for the CZTS and hybrid CZTS-Based solar cells, respectively. Thus, the appreciable increment in the efficiency values of hybrid CZTS solar cells showed the positive performance of the sandwich absorber layer.

Funding

This research received no external funding.

Acknowledgments

The authors will also like to appreciate Prof. Marc. Burgelman and his co-researchers at the University of Gents, Belgium, for making SCAPS-1D available for use.

Conflicts of Interest

The authors declared no conflict of interest.

References

1. Boehman, A.L.; Maroto-Valer, M.M.; Scaroni, A.W.; Schobert, H.H. Fossil and renewable fuels challenges for the 21st century. *ACS Natl. Meet. B. Abstr.* **2004**, *228*, 724–727.
2. Chand Malav, L.; Yadav, K.K.; Gupta, N.; Kumar, S.; Sharma, G.K.; Krishnan, S.; Rezania, S.; Kamyab, H.; Pham, Q.B.; Yadav, S.; et al. A review on municipal solid waste as a renewable source for waste-to-energy project in India: Current practices, challenges, and future opportunities. *J. Clean. Prod.* **2020**, *277*, 123227, https://doi.org/10.1016/j.jclepro.2020.123227.
3. Abomohra, A.E.F.; Elsayed, M.; Esakkimuthu, S.; El-Sheekh, M.; Hanelt, D. Potential of fat, oil and grease (FOG) for biodiesel production: A critical review on the recent progress and future perspectives. *Prog. Energy Combust. Sci.* **2020**, *81*, 100868, https://doi.org/10.1016/j.pecs.2020.100868.
4. Kan, A.; Zeng, Y.; Meng, X.; Wang, D.; Xina, J.; Yang, X.; Tesren, L. The linkage between renewable energy potential and sustainable development: Understanding solar energy variability and photovoltaic power potential in Tibet, China. *Sustain. Energy Technol. Assessments* **2021**, *48*, 101551, https://doi.org/10.1016/j.seta.2021.101551.
5. Sengupta, M.; Habte, A.; Wilbert, S.; Gueymard, C.; Remund, J. Best Practices Handbook for the Collection and Use of Solar Resource Data for Solar Energy Applications: Third Edition. **2021**, 1–348, https://iea-pvps.org/key-topics/best-practices-handbook-for-the-collection-and-use-of-solar-resource-data-for-solar-energy-applications-third-edition/.
6. Vaithilingam, S.; Gopal, S.T.; Srinivasan, S.K.; Manokar, A.M.; Sathyamurthy, R.; Esakkimuthu, G.S.; Kumar, R.; Sharifpur, M. An extensive review on thermodynamic aspect based solar desalination techniques. *J. Therm. Anal. Calorim.* **2021**, *145*, 1103–1119, https://doi.org/10.1007/s10973-020-10269-x.
7. Pareek, A.; Dom, R.; Gupta, J.; Chandran, J.; Adepu, V.; Borse, P.H. Insights into renewable hydrogen energy: Recent advances and prospects. *Mater. Sci. Energy Technol.* **2020**, *3*, 319–327, https://doi.org/10.1016/j.mset.2019.12.002.
8. Aslam, A.; Mehmood, U.; Arshad, M.H.; Ishfaq, A.; Zaheer, J.; Ul Haq Khan, A.; Sufyan, M. Dye-sensitized solar cells (DSSCs) as a potential photovoltaic technology for the self-powered internet of things (IoTs) applications. *Sol. Energy* **2020**, *207*, 874–892, https://doi.org/10.1016/j.solener.2020.07.029.
9. Ansari, A.A.; Nazeeruddin, M.K.; Tavakoli, M.M. Organic-inorganic upconversion nanoparticles hybrid in dye-sensitized solar cells. *Coord. Chem. Rev.* **2021**, *436*, 213805, https://doi.org/10.1016/j.ccr.2021.213805.
10. Sabzyan, H.; Ghaderi, F. Evaluation of the optical properties of the lead-free mixed-halide iron perovskite CH3NH3FeI2Br for application in solar cells: A computational study. *Mater. Today Commun.* **2021**, *26*, 101847, https://doi.org/10.1016/j.mtcomm.2020.101847.
11. Ki, W.; Hillhouse, H.W. Earth-abundant element photovoltaics directly from soluble precursors with high yield using a non-toxic solvent. *Adv. Energy Mater.* **2011**, *1*, 732–735, https://doi.org/10.1002/aenm.201100140.
12. Sharmin, A.; Bashar, M.S.; Sultana, M.; Al Mamun, S.M.M. Sputtered single-phase kesterite Cu2ZnSnS4 (CZTS) thin film for photovoltaic applications: Post annealing parameter optimization and property analysis. *AIP Adv.* **2020**, *10*, https://doi.org/10.1063/1.5129202.
13. Elhmaidi, Z.O.; Abd-Lefdil, M.; Khakani, M.A. El Photoconversion optimization of pulsed-laser-deposited p-CZTS/n-Si-nanowires heterojunction-based photovoltaic devices. *Nanomaterials* **2020**, *10*, 1–14, https://doi.org/10.3390/nano10071393.
14. Katagiri, H.; Jimbo, K.; Maw, W.S.; Oishi, K.; Yamazaki, M.; Araki, H.; Takeuchi, A. Development of CZTS-based thin film solar cells. *Thin Solid Films* **2009**, *517*, 2455–2460, https://doi.org/10.1016/j.tsf.2008.11.002.

15. Sava, F.; Diagne, O.; Galca, A.; Simandan, I.; Matei, E.; Burdusel, M.; Becherescu, N.; Becherescu, V.; Mihai, C.; Velea, A. Secondary Crystalline Phases Influence on Optical Properties in Off-Stoichiometric Cu2S–ZnS–SnS2 Thin Films. *Materials (Basel).* **2020**, *4*, 1–14, https://doi.org/10.3390/ma13204624.
16. Shin, B.; Gunawan, O.; Zhu, Y.; Bojarczuk, N.A.; Chey, S.J.; Guha, S. Thin film solar cell with 8.4% power conversion efficiency using an earth-abundant Cu2ZnSnS4 absorber. *Prog. PHOTOVOLTAICS Res. Appl.* **2013**, *21*, 72–76, https://doi.org/10.1002/pip.1174.
17. Gezgin, S.Y.; Houimi, A.; Mercimek, B.; Kiliç, H.Ş. The Effect of CZTS Ultrathin Film Thickness on the Electrical Characteristic of CZTS/Si Heterojunction Solar Cells in the Darkness and under the Illumination Conditions. *Silicon* **2021**, *13*, 3555–3567, https://doi.org/10.1007/s12633-020-00847-x.
18. Mkawi, E.M.; Al-Hadeethi, Y.; Shalaan, E.; Bekyarova, E. Solution-processed sphere-like Cu2ZnSnS4 nanoparticles for solar cells: effect of oleylamine concentration on properties. *Appl. Phys. A Mater. Sci. Process.* **2020**, *126*, 1–8, https://doi.org/10.1007/s00339-019-3233-1.
19. Jackson, P.; Hariskos, D.; Lotter, E.; Paetel, S.; Wuerz, R.; Menner, R.; Wischmann, W.; Powalla, M. New world record efficiency for Cu(In,Ga)Se2 thin-film solar cells beyond 20%. *Prog. Photovoltaics Res. Appl.* **2011**, *19*, 894–897, https://doi.org/10.1002/pip.1078.
20. Lee, M.M.; Teuscher, J.; Miyasaka, T.; Murakami, T.N.; Snaith, H.J. Efficient hybrid solar cells based on meso-superstructured organometal halide perovskites. *Science (80-.).* **2012**, *338*, 643–647, https://doi.org/10.1126/science.1228604.
21. Burschka, J.; Pellet, N.; Moon, S.J.; Humphry-Baker, R.; Gao, P.; Nazeeruddin, M.K.; Grätzel, M. Sequential deposition as a route to high-performance perovskite-sensitized solar cells. *Nature* **2013**, *499*, 316–319, https://doi.org/10.1038/nature12340.
22. Liu, M.; Johnston, M.B.; Snaith, H.J. Efficient planar heterojunction perovskite solar cells by vapour deposition. *Nature* **2013**, *501*, 395–398, https://doi.org/10.1038/nature12509.
23. Grätzel, M. The light and shade of perovskite solar cells. *Nat. Mater.* **2014**, *13*, 838–842, https://doi.org/10.1038/nmat4065.
24. Suarez, B.; Gonzalez-Pedro, V.; Ripolles, T.S.; Sanchez, R.S.; Otero, L.; Mora-Sero, I. Recombination study of combined halides (Cl, Br, I) perovskite solar cells. *J. Phys. Chem. Lett.* **2014**, *5*, 1628–1635, https://doi.org/10.1021/jz5006797.
25. Deschler, F.; Price, M.; Pathak, S.; Klintberg, L.E.; Jarausch, D.D.; Higler, R.; Hüttner, S.; Leijtens, T.; Stranks, S.D.; Snaith, H.J.; et al. High photoluminescence efficiency and optically pumped lasing in solution-processed mixed halide perovskite semiconductors. *J. Phys. Chem. Lett.* **2014**, *5*, 1421–1426, https://doi.org/10.1021/jz5005285.
26. Xing, G.; Mathews, N.; Lim, S.S.; Yantara, N.; Liu, X.; Sabba, D.; Grätzel, M.; Mhaisalkar, S.; Sum, T.C. Low-temperature solution-processed wavelength-tunable perovskites for lasing. *Nat. Mater.* **2014**, *13*, 476–480, https://doi.org/10.1038/nmat3911.
27. Zhou, H.; Chen, Q.; Li, G.; Luo, S.; Song, T.B.; Duan, H.S.; Hong, Z.; You, J.; Liu, Y.; Yang, Y. Interface engineering of highly efficient perovskite solar cells. *Science (80-.).* **2014**, *345*, 542–546, https://doi.org/10.1126/science.1254050.
28. Bello, I.T.; Odedunmoye, Y.A.; Adedokun, O.; Shittu, H.A.; Awodugba, A.O. Numerical Simulation of Sandwiched Perovskite-Based Solar Cell Using Solar Cell Capacitance Simulator (SCAPS-1D). *J. Niger. Soc. Phys. Sci.* **2019**, *1*, 57–61, https://doi.org/10.46481/jnsps.2019.11.
29. Uzum, A. Device simulations of electron-transfer-layer-free perovskite solar cells focused on absorber/hole transfer-layer interface. *Semicond. Sci. Technol.* **2021**, *36*, https://doi.org/10.1088/1361-6641/ac01fd.
30. Burgelman, M.; Decock, K.; Niemegeers, A.; Verschraegen, J.; Degrave, S. SCAPS Manual. *Univ. Gent* **2019**, 1–111, https://users.elis.ugent.be/ELISgroups/solar/projects/scaps/SCAPS%20manual%20most%20recent.pdf.
31. Nalianya, M.A.; Awino, C.; Barasa, H.; Odari, V.; Gaitho, F.; Omogo, B.; Mageto, M. Numerical study of lead free CsSn0.5Ge0.5I3 perovskite solar cell by SCAPS-1D. *Optik (Stuttg).* **2021**, *248*, 168060, https://doi.org/10.1016/j.ijleo.2021.168060.
32. Minemoto, T.; Murata, M. Device modeling of perovskite solar cells based on structural similarity with thin film inorganic semiconductor solar cells. *J. Appl. Phys.* **2014**, *116*, 1–6, https://doi.org/10.1063/1.4891982.
33. Gloeckler, M.; Fahrenbruch, A.L.; Sites, J.R. Numerical modeling of CIGS and CdTe solar cells: Setting the baseline. *Proc. 3rd World Conf. Photovolt. Energy Convers.* **2003**, *A*, 491–494, https://ieeexplore.ieee.org/document/1305328.

34. Wang, D.; Wright, M.; Elumalai, N.K.; Uddin, A. Stability of perovskite solar cells. *Sol. Energy Mater. Sol. Cells* **2016**, *147*, 255–275, https://doi.org/10.1016/j.solmat.2015.12.025.
35. Chen, Q.; De Marco, N.; Yang, Y.; Song, T. Bin; Chen, C.C.; Zhao, H.; Hong, Z.; Zhou, H.; Yang, Y. Under the spotlight: The organic-inorganic hybrid halide perovskite for optoelectronic applications. *Nano Today* **2015**, *10*, 355–396, https://doi.org/10.1016/j.nantod.2015.04.009.
36. Fonash, S.J. *Solar Cell Device Physics*; 2nd Editio.; Elsevier Inc., 2010; ISBN 9781119130536, https://www.elsevier.com/books/solar-cell-device-physics/fonash/978-0-12-374774-7.
37. Shockley, W.; Queisser, H.J. Detailed balance limit of efficiency of p-n junction solar cells. *J. Appl. Phys.* **1961**, *32*, 510–519, https://doi.org/10.1063/1.1736034.
38. Bello, I.T.; Awodele, M.K.; Adedokun, O.; Akinrinola, O.; Awodugba, A.O. Modeling and simulation of CZTS-perovskite sandwiched tandem solar cell. *Turkish J. Phys.* **2018**, *42*, 321–328, https://doi.org/10.3906/fiz-1801-30.